RSC Advances

PAPER

View Article Online
View Journal | View Issue

Cite this: *RSC Adv.*, 2017, **7**, 32419

Theoretical insights into the reaction mechanism between tetrachloro-*o*-benzoquinone and *N*-methyl benzohydroxamic acid†

Weihua Wang,*[a] Chao Guo,[a] Wenling Feng,[a] Qiao Sun[b] and Ping Li*[a]

Acquiring the detailed reaction mechanism between halogenated quinones and hydroxamic acids is crucial for better understanding of the potential applications of benzohydroxamic acids in the detoxification of the carcinogenic polyhalogenated quinoid metabolites of pentachlorophenol. In this study, the reaction mechanism between tetrachloro-*o*-benzoquinone (*o*-TCBQ) and *N*-methyl benzohydroxamic acid (*N*-MeBHA) has been systematically investigated at the B3LYP/6-311++G(d,p) level. It was found that *o*-TCBQ can react with the anion of *N*-MeBHA (*N*-MeBHA$^-$) under mild conditions. As the first step of reaction, a molecular complex is formed between *o*-TCBQ and *N*-MeBHA$^-$ followed by the nucleophilic attack of the O atom of *N*-MeBHA$^-$ at the C atom attached to the Cl atom of *o*-TCBQ, resulting in the formation of an unstable intermediate containing an N–O bond. Subsequently, the unstable intermediate decomposes *via* the homolytic cleavage of the N–O bond to produce N-centered and O-centered radicals. For the O-centered radical, it can isomerize to a C-centered form upon structural relaxation. Finally, these radicals react with each other to form the major C–N bonding products and minor C–O bonding products. In addition, it was found that the reactivity of *o*-TCBQ with *N*-MeBHA is higher than that of tetrachloro-*p*-benzoquinone (*p*-TCBQ).

Received 5th May 2017
Accepted 16th June 2017

DOI: 10.1039/c7ra05083f

rsc.li/rsc-advances

1. Introduction

As the major genotoxic and carcinogenic quinoid metabolites of the widely used wood preservative pentachlorophenol (PCP), polyhalogenated quinones can create many hazardous effects *in vivo*, *e.g.*, acute hepatotoxicity, nephrotoxicity, and carcinogenesis,[1,2] where PCP has been classified as a group 2B environmental carcinogen by the International Association for Research on Cancer. Meanwhile, halogenated quinones can also be produced during the oxidation or destruction of polyhalogenated persistent organic pollutants (POPs).[3–5] In particular, some halobenzoquinones have been identified as an emerging class of disinfection byproducts in drinking water.[6–8] More recently, it was found that the polyhalogenated quinones can react with hydrogen peroxide (H_2O_2) or organic hydroperoxides to produce hydroxyl and alkoxyl radicals experimentally,[9–16] which can partially explain the potential carcinogenicity of polyhalogenated aromatic environmental pollutants.

Another species of environmental and biomedical interest are hydroxamic acids, which have been paid extensive attention due to their strong capacity to inhibit transition-metal-mediated oxidative stress and the activity of many enzymes (*e.g.*, metalloproteases and lipoxygenase).[17–19] Clinically, the suberoylanilide hydroxamic acid and deferoxamine have been applied for the treatment of cancer and iron-overload diseases. Moreover, hydroxamic acids can effectively detoxify the carcinogenic polyhalogenated quinoid metabolites of pentachlorophenol and other persistent organic pollutants.[20–22] For example, benzohydroxamic acid can dramatically accelerate the conversion of the highly toxic tetrachloro-*p*-benzoquinone (*p*-TCBQ) to much less toxic chloranilic acid *via* an unusual double Lossen rearrangement mechanism.[20] However, for the *N*-methyl benzohydroxamic acid, it can react with 2,5-dichloro-1,4-benzoquinone (DCBQ) through a radical mechanism.[21,22] Namely, a nucleophilic reaction may take place between DCBQ and *N*-MeBHA to form a relatively stable initial product followed by its homolytic decomposition to produce N- and O-centered radicals. Especially, for the N-centered radical, it can readily attack the deoxynucleotides, exhibiting its potential biological implications.[22] For the O-centered radical, it can isomerize to the C-centered radical, which can be further coupled with the N-centered radical to produce the major C–N bonding product *via* keto–enol tautomerization. Similarly, the same is also true for the *p*-TCBQ although no keto–enol tautomerization products have been observed due to the specific geometry of *p*-TCBQ.[22]

[a]*Key Laboratory of Life-Organic Analysis, School of Chemistry and Chemical Engineering, Qufu Normal University, Qufu, 273165, P. R. China. E-mail: wwh78@163.com; lignip@163.com*

[b]*Collaborative Innovation Center of Radiation Medicine of Jiangsu Higher Education Institutions, School for Radiological and Interdisciplinary Sciences, Soochow University, Suzhou, 215123, P. R. China*

† Electronic supplementary information (ESI) available. See DOI: 10.1039/c7ra05083f

As the isomer of *p*-TCBQ and another quinoid metabolites of PCP, *o*-TCBQ has been involved in the toxicity of the bleached kraft chlorination effluent many years ago.[23] However, *o*-TCBQ has been paid less attention compared with the *p*-TCBQ.[24–30] Can it react with *N*-MeBHA similar to that of *p*-TCBQ? If so, what is the detailed reaction mechanism? What are the final reaction products? Obviously, the clarifications of these questions are crucial for the understanding of the reactivity of *ortho*-halogenated benzoquinones with *N*-MeBHA as well as the detoxification of the benzohydroxamic acids. Unfortunately, these questions have not been clarified to the best of our knowledge. So, a theoretical investigation on the title reaction appears to be highly desirable in the lack of the relevant experimental studies.

Therefore, to address these questions mentioned above, in this study, the reaction mechanism between *o*-TCBQ and *N*-MeBHA has been systematically investigated employing the density functional theory (DFT) method. As a result, the detailed reaction mechanism for the title reaction has been clarified at the electronic level. Besides the major C–N bonding products, the minor C–O bonding products have also been observed. Expectedly, the present results not only can provide scientific proof for the detection and identification of the relevant products of the title reaction, but also can provide useful clues to the design and synthesis of large-size molecules containing C–N bond experimentally.

2. Computational methods

All the species in the whole reaction have been fully optimized at the B3LYP/6-311++G(d,p) level, where the reliability and efficiency of the method in predicting geometries and properties has been verified by a number of systems.[31–39] Subsequently, vibrational frequency analysis has been performed at the same level to identify the nature of the optimized structures. Moreover, intrinsic reaction coordinate (IRC)[40,41] calculations were performed to further verify that the calculated transition states indeed connected the reactants and products, where the selected results have been given in Fig. S1 of the ESI† for reference.

To further testify the reliability of the B3LYP functional, the relevant calculations for the reaction of *o*-TCBQ with neutral *N*-MeBHA in the presence of one water molecule and the direct reaction of *o*-TCBQ with the anion of *N*-MeBHA have been performed at the M06/6-311++G(d,p) level. As a result, it was found that the calculated results including geometries and energy barriers are consistent with each other at both levels. For the sake of simplicity, the relevant discussions have been given in the ESI† for reference.

To calculate the interaction energy between free radicals, the Boys–Bernardi counterpoise technique has been employed to evaluate the basis set superposition errors (BSSE).[42]

To investigate the solvent effect on the nucleophilic attack process of *N*-MeBHA to *o*-TCBQ, the polarizable continuum model (PCM)[43,44] was employed in aqueous solution within the framework of self-consistent reaction filed (SCRF) theory. To explore the possibility of the proceeding of the title reaction in the presence of water molecules, different numbers of explicit water molecules ranging from one to three have been introduced to assist the proton transfer process.

To qualitatively predict which bond to be dissociated in the formed intermediate, *ab initio* molecular dynamics has been carried out at the B3LYP/6-311G(d,p) level using the atom-centered density matrix propagation (ADMP) molecular dynamics.[45–47] The dynamics calculations were performed under condition of constant temperature at 298.15 K. The simulation time is long enough to observe the necessary phenomena with a time step of 0.5 fs.

All the calculations have been carried out using Gaussian 09 program.[48]

3. Results and discussion

In realistic system, *N*-MeBHA should exist in its neutral and anionic forms depending on the pH of solution. So the reactions of *o*-TCBQ with neutral and anionic *N*-MeBHA have been investigated, respectively.

For the sake of simplicity, the symbols MC, IM, TS, and P have been employed to stand for the optimized molecular complexes, intermediates, transition states, and products, respectively. All the Cartesian coordinates of the optimized species have been given in the ESI† for reference.

3.1 The reaction of *o*-TCBQ with neutral *N*-MeBHA

Firstly, the reaction of *o*-TCBQ with neutral *N*-MeBHA has been investigated. Similar to the reactions of *p*-TCBQ and *o*-TCBQ with H_2O_2,[30,49] the nucleophilic attack process of *N*-MeBHA to *o*-TCBQ has been mainly explored. As shown in Fig. 1, four reaction modes, namely N1, N2, N3, and N4, have been constructed considering the symmetry of *o*-TCBQ. A molecular complex MC1 has been located as the first step of the reaction. Moreover, MC1 acts as the common reactant for the four reaction modes, which has been confirmed by the IRC calculations. Subsequently, nucleophilic attack of the hydroxyl O atom of *N*-MeBHA to the C atom attached to the Cl atom of *o*-TCBQ occurs, accompanying with the proton transfer from *N*-MeBHA to the Cl atom attached to the attacked C atom of *o*-TCBQ. After then, an intermediate containing N–O bond has been produced. As presented in Table 1, the MC1 has been stabilized by about 4.12 kcal mol^{-1}. The energy barriers in the nucleophilic attack processes range from 50.71 to 51.33 kcal mol^{-1} relative to the separated reactants, implying that it is difficult to occur for the reaction between *o*-TCBQ and neutral *N*-MeBHA. Moreover, the calculated Gibbs free energy changes for the formation processes of the intermediates are positive values, suggesting that the whole processes are unfavorable thermodynamically.

Moreover, given the positive catalytic role of water molecules in the assistance of proton transfer, so the reaction of *o*-TCBQ with *N*-MeBHA with the assistance water molecules have been investigated on the basis of the N3 reaction mode. As displayed in Fig. 2, one, two, and three water molecules have been introduced to assist the proton transfer mentioned above. Here, the bridge role of water molecules in the assistance of proton transfer should be highlighted. For example, the introduced

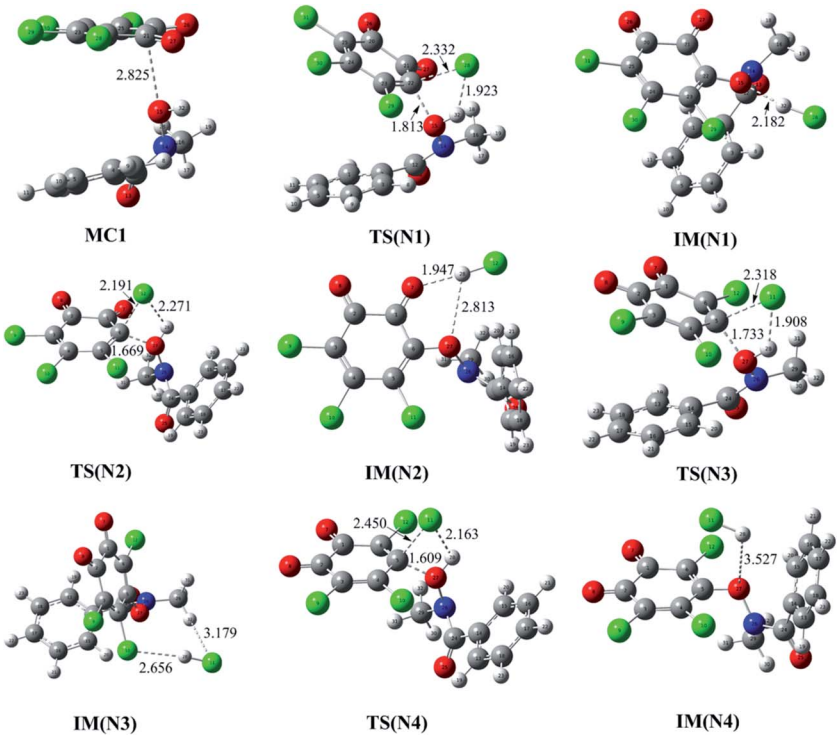

Fig. 1 Optimized molecular complexes (MC), transition states (TS), and intermediates (IM) in the different reaction modes of *o*-TCBQ with isolated neutral *N*-MeBHA. The selected interatomic distances are given in Å.

Table 1 Calculated energy parameters for the direct nucleophilic attack of *N*-MeBHA to *o*-TCBQ relative to the separated reactants[a]

Attack modes	MC	TS	IM
N1	−4.12	51.33	−1.15/−0.14/8.72
N2	−4.12	50.78	−2.10/−1.38/8.30
N3	−4.12 (−13.68/−22.78/ −27.03)	50.71 (40.03/27.76/ 18.21)	−1.29/−0.04/6.23 (−12.34/−13.08/ −23.10)
N4	−4.12	51.00	−1.55/−0.45/8.34

[a] All the units are in kcal mol^{-1}. The data before and after slash refer to the relative energies, enthalpy changes, and Gibbs free energy changes, respectively. The data in parentheses refer to the results involving one, two, and three water molecules, respectively.

single water molecule can accept the hydroxyl proton of *N*-MeBHA and gives its own proton to the dissociated Cl atom of *o*-TCBQ simultaneously. Similarly, the same is also true if a second/third water molecule is introduced, where the second/third water molecule accepts the proton of the first/second water molecule and give its proton to the Cl atom of *o*-TCBQ. As presented in Table 1, compared with the case without involving water molecules, the energy barriers in the nucleophilic attack process have been reduced by 10.68, 22.95, and 32.50 kcal mol^{-1} to 40.03, 27.76, and 18.21 kcal mol^{-1} in the assistance of one, two, and three water molecules, respectively. Despite the positive catalytic role of water molecules in reducing the energy barrier, the energy barrier here is still so high that the title reaction is difficult to occur under normal conditions.

3.2 The reaction of *o*-TCBQ with *N*-MeBHA anion

As mentioned above, the reaction of *o*-TCBQ with neutral *N*-MeBHA is difficult to take place regardless of the presence of explicit water molecules or not. Given the fact that *N*-MeBHA$^-$ anion can be produced from the acid–base dissociation equilibrium of *N*-MeBHA and it is a better nucleophile than neutral *N*-MeBHA, the direct reaction between *o*-TCBQ and *N*-MeBHA$^-$ has been investigated below to further clarify the reactivity of the title reaction.

3.2.1 The formation of molecular complexes. As shown in Fig. 3, four reaction modes named as A1, A2, A3, and A4 have been constructed for the reaction of *o*-TCBQ with *N*-MeBHA$^-$. Similar to the reaction involving neutral *N*-MeBHA, molecular complexes have also been located as the first step of the reaction, which are further confirmed by the IRC calculations.

As presented in Table 2, these MCs have been significantly stabilized ranging from 29.44 to 32.24 kcal mol^{-1} relative to the separated reactants, which are much larger than those of the MCs in the reactions involving neutral *N*-MeBHA. Moreover, the formation of these MCs is favorable exothermic and spontaneous process thermodynamically from the calculated negative values of the enthalpy and Gibbs free energy changes.

3.2.2 The nucleophilic attack process. As displayed in Fig. 3, the O atom of *N*-MeBHA$^-$ can directly attack the C atom attached to the Cl atom of *o*-TCBQ. Unlike the reaction involving neutral *N*-MeBHA, all the transition states here are lower in

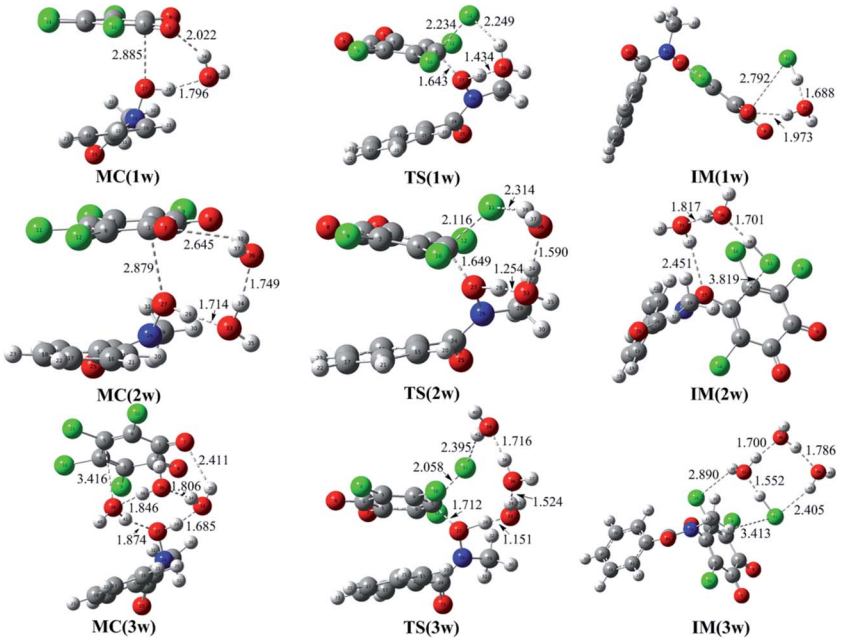

Fig. 2 Optimized molecular complexes (MC), transition states (TS), and intermediates (IM) in the reaction of *o*-TCBQ with neutral *N*-MeBHA in the assistance of water molecules. The selected interatomic distances are given in Å.

energy by 22.94–25.93 kcal mol^{-1} than the separated reactants. As a result, depending on the specific reaction mode, the energy barriers in the nucleophilic attack processes are in the range of 3.51–8.79 kcal mol^{-1} relative to that of the corresponding MC. Obviously, it is easy to take place for the reaction of *o*-TCBQ with *N*-MeBHA^{-}. Actually, for the reaction of *p*-TCBQ with benzohydroxamic acid, it was also found that the free benzohydroxamate anion is essential for the dramatic acceleration of *p*-TCBQ hydrolysis.[20] As for the nucleophilic attacked products, *i.e.*, the intermediates containing N–O bond, they have been significantly stabilized by 36.02–39.33 kcal mol^{-1}. Moreover, the enthalpy and Gibbs free energy changes are all negative values in the formation processes of these intermediates, where the former and the latter range from −35.52 to −38.84 kcal mol^{-1} and from −23.92 to −27.72 kcal mol^{-1}, respectively. Therefore, the reaction of *o*-TCBQ with *N*-MeBHA^{-} is more favourable than that of the reaction involving neutral *N*-MeBHA thermodynamically and kinetically.

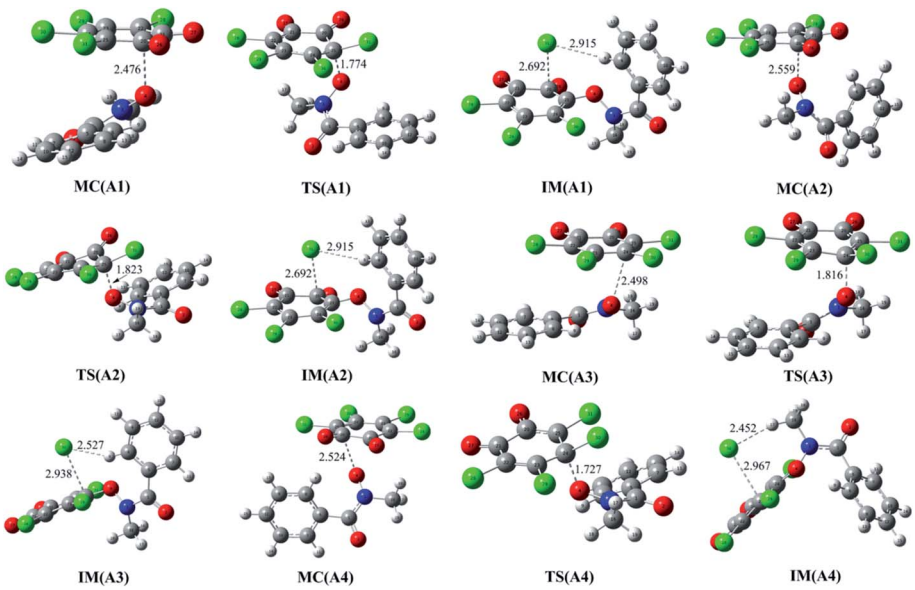

Fig. 3 Optimized molecular complexes (MC), transition states (TS), and intermediates (IM) in the different reaction modes of *o*-TCBQ with *N*-MeBHA^{-}. The selected interatomic distances are given in Å.

Table 2 Calculated relative energies (Δ*E*), enthalpy changes (Δ*H*), and Gibbs free energy changes (Δ*G*) for the available molecular complexes, transition states, and intermediates in the nucleophilic attack of *N*-MeBHA$^-$ to *o*-TCBQ relative to the separated reactants[a]

Attack modes	MC	TS	IM
A1	−32.24/−31.76/−19.99	−24.30	−39.33/−38.84/−27.71
A2	−31.73/−31.18/−20.00	−22.94	−39.33/−38.34/−27.72
A3	−29.44/−29.04/−16.69	−25.93	−36.02/−35.52/−23.92
	(−9.55)	(−6.51)	(−28.62/−27.92/−19.56)
A4	−31.73/−31.18/−20.00	−23.05	−38.38/−37.80/−26.62
p-A1	−29.39	−20.97	−38.32/−37.83/−26.14
p-A2	−29.35	−21.38	−38.94/−38.48/−26.55
	(−9.86)	(−1.51)	(−29.44/−28.75/−21.08)

[a] All the units are in kcal mol^{-1}. The data before and after slash refer to the relative energies, enthalpy changes, and Gibbs free energy changes, respectively. The data in parentheses refer to the corresponding results in aqueous solution.

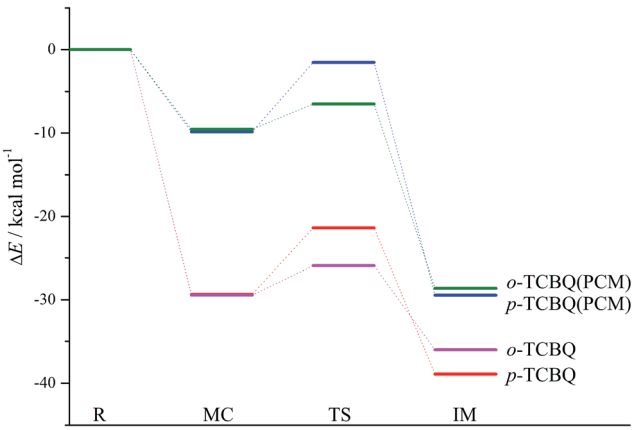

Fig. 5 The reaction profiles for the nucleophilic attack processes of *N*-MeBHA$^-$ to *o*-TCBQ and *p*-TCBQ in the gas phase and in aqueous solution.

Moreover, given the fact that the reaction takes place in solution generally, so the solvent effect on the above reaction has been included on the basis of the reaction mode A3 possessing the lowest energy barrier. As a result, the original energy barrier has been increased by about 19.42 kcal mol^{-1} in aqueous solution, which is still lower by 6.51 kcal mol^{-1} in energy relative to the separated reactants. Actually, the energy barrier is only 3.04 kcal mol^{-1} relative to the molecular complex, which is comparable to that of the reaction of *o*-TCBQ with H_2O_2.[30] Therefore, it is easy to occur for the title reaction in solution.

In addition, the reaction of *p*-TCBQ with *N*-MeBHA$^-$ has also been investigated for comparison. Similar to *o*-TCBQ, as shown in Fig. 4, the corresponding molecular complexes and transition states have also been located, where two reaction modes (*p*-A1 and *p*-A2) have been constructed due to the symmetry of *p*-TCBQ. As presented in Table 2, the energy barriers for *p*-A1 and *p*-A2 are −20.97 and −21.38 kcal mol^{-1} relative to the separated reactants. Moreover, the energy barrier has been increased to −1.51 kcal mol^{-1} if solvent effect is considered. Here, the low barrier is consistent with the fact that *p*-TCBQ can readily react with *N*-MeBHA under mild conditions.[22] For comparison, the reaction profiles for the reactions of *N*-MeBHA$^-$ with *o*-TCBQ and *p*-TCBQ have been shown in Fig. 5. Obviously, the lower energy barrier for the reaction of *N*-MeBHA$^-$ with *o*-TCBQ suggests its higher reactivity than that of *p*-TCBQ.

3.2.3 The formation of radicals. To qualitatively predict which bond to be dissociated in the formed intermediate after the dissociation of the Cl$^-$, *ab initio* molecular dynamics has been performed firstly on the basis of the IM(A2). As displayed in Fig. 6, the newly formed C25–O4 bond changes equably nearby its original equilibrium distance overall. However, for the N3–O4 bond adjacent to the C25–O4 bond significantly deviates from its equilibrium distance in the most of dynamical time, exhibiting the weakness of the N3–O4 bond.

Subsequently, to confirm the decomposition mode of N3–O4 bond, its bond decomposition enthalpy (BDE) has been

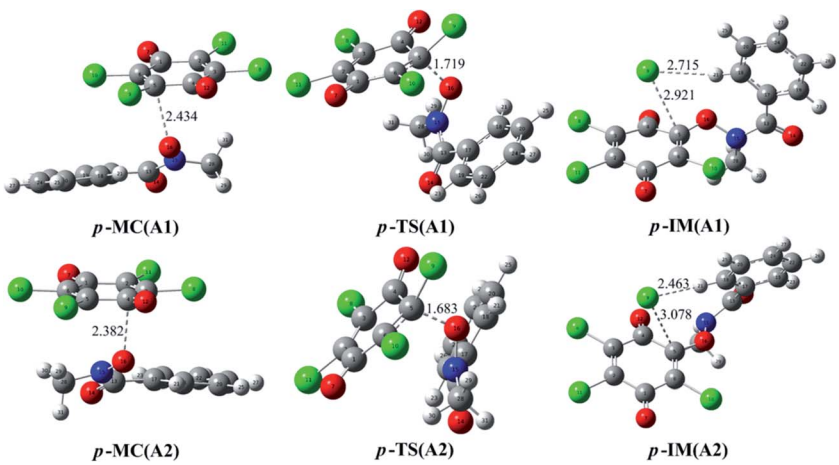

Fig. 4 Optimized molecular complexes (MC), transition states (TS), and intermediates (IM) in the different reaction modes of *p*-TCBQ with *N*-MeBHA$^-$. The selected interatomic distances are given in Å.

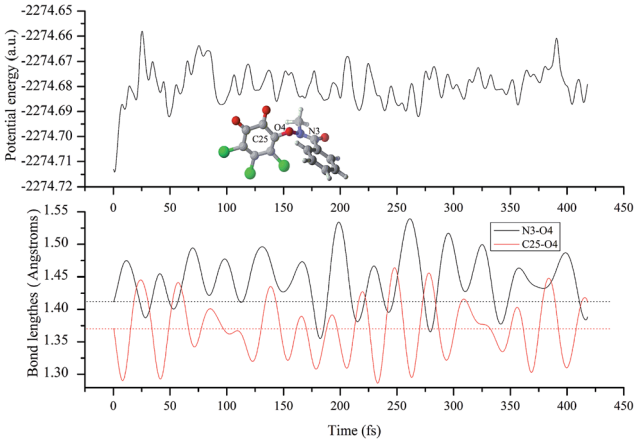

Fig. 6 The variations of the potential energy and selected bond lengthes during the molecular dynamics for IM(A2) after the dissociation of Cl^-. The dotted lines refer to the equilibrium distances in IM(A2).

investigated on the basis of the IM(A2) since no transition state has been located for the cleavage of the N3–O4 bond. For the heterolytic cleavage of the N–O bond, the BDE is 140.82 and 165.23 kcal mol^{-1} for the decomposed species between N^+ and O^- fragments or the N^- and O^+ fragments, where the corresponding geometries have been given in Fig. S2 of the ESI† for reference. However, for the homolytic cleavage of the N–O bond, the BDE is only 6.50 kcal mol^{-1}, which is much smaller than that of the heterolytic cleavage. Therefore, the decomposition of IM should occur *via* the homolytic cleavage of the N–O bond. For the sake of simplicity, the produced N- and O-centered radicals are named as $^{\bullet}N(CH_3)$–COAr and *o*-CBQ$^{\bullet}$, respectively.

As displayed in Fig. 7, for the $^{\bullet}N(CH_3)$–COAr radical, the unpaired electron is mainly distributed around the N atom before and after structural relaxation. At the same time, small amounts of the unpaired electron have also been observed on the O atom. As for the *o*-CBQ$^{\bullet}$ radical, the spin density

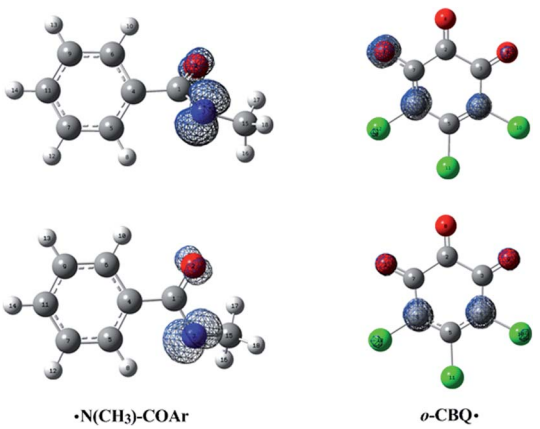

Fig. 7 Spin density maps for the free radicals before and after structural relaxation (top and bottom) in the homolytic cleavage of the N–O bond of IM(A2) after the dissociation of Cl^-. The isodensity contours are 0.01 electron $bohr^{-3}$.

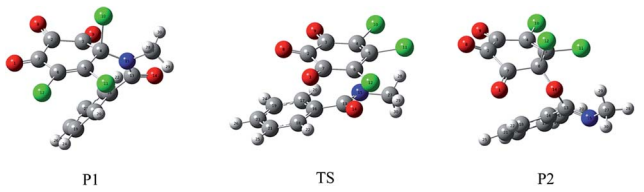

Fig. 8 The formed C–N bonding and C–O bonding products for the title reaction and the transition state between them.

redistribution from the O atom involved in the N–O cleavage to its adjacent C* atom attached to the Cl atom occurs upon structural relaxation. Therefore, the N and O atoms in $^{\bullet}N(CH_3)$–COAr radical and the C* atom in *o*-CBQ$^{\bullet}$ radical should be the active sites for the subsequent reactions.

3.2.4 The formation of the reaction products. On the basis of the spin density analyses mentioned above, the possible reaction products have been constructed. As shown in Fig. 8, not only the C–N bonding product P1, but also the C–O bonding product P2 has also been located. As presented in Table 3, the interaction energies are −31.17 and −17.10 kcal mol^{-1} for P1 and P2, respectively. Correspondingly, P1 is more stable by 14.53 kcal mol^{-1} than P2. The calculated enthalpy and Gibbs free energy changes are all negative values, suggesting that the formation processes of P1 and P2 are exothermic and spontaneous reactions. Meanwhile, the more negative value of Gibbs free energy changes for P1 implies that the formation of P1 is more favorable than that of P2 thermodynamically.

Moreover, as shown in Fig. 8, a transition state has been located between P1 and P2, which is confirmed by the IRC calculation. The forward and reverse energy barriers are 43.04 and 28.52 kcal mol^{-1}, where the direction from P1 to P2 is defined as the forward reaction. Obviously, it is difficult to interconvert between P1 and P2. Given the fact that no transition state has been observed in the formation processes of P1 and P2, so the major products for the title reaction should be the C–N bonding types as well as the minor C–O bonding types.

On the basis of the above analyses, the reaction mechanism for the title reaction can be summarized as follows. As shown in Fig. 9, *o*-TCBQ can react with the anionic form of the *N*-MeBHA. As the first step of the reaction, a molecular complex has been formed followed by the nucleophilic attack of *N*-MeBHA$^-$ to *o*-TCBQ to form an unstable intermediate containing N–O bond. After that, the unstable intermediate decomposes homolytically *via* the N–O bond to form the N- and O-centered radicals. For the O-centered radical, it can isomerize to the C-centered radical upon structural relaxation. Finally, these radicals

Table 3 Calculated energy parameters for the reaction products formed between *o*-CBQ$^{\bullet}$ and $^{\bullet}N(CH_3)$–COAr radicals[a]

Complexes	ΔE_{Int}	ΔH	ΔG	ΔE_{Rel}
P1	−31.17	−36.07	−20.12	0.00
P2	−17.10	−21.27	−6.34	14.53

[a] All the units are in kcal mol^{-1}.

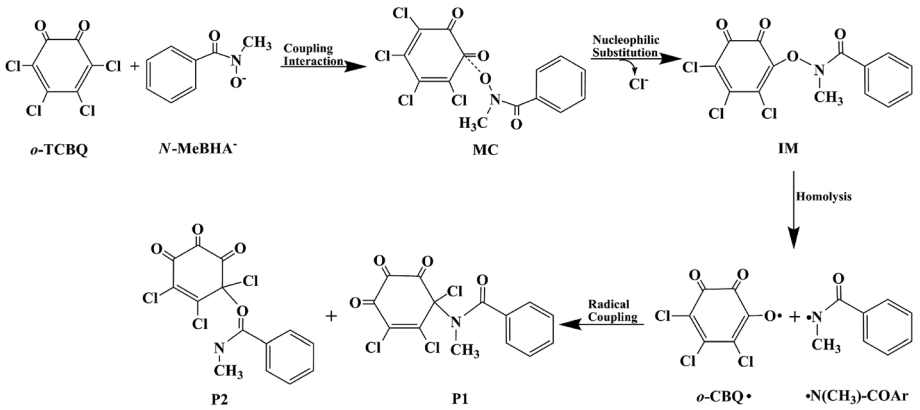

Fig. 9 The proposed reaction mechanism for the reaction of *o*-TCBQ with *N*-MeBHA$^-$.

interact with each other to form the C–N bonding products predominately as well as minor C–O bonding products. Certainly, relevant experiments are required to confirm the present results.

4. Conclusions

In this study, the reaction mechanism between *o*-TCBQ and *N*-MeBHA has been systematically investigated at the B3LYP/6-311++G(d,p) level. It was found that *o*-TCBQ can directly react with the anion of *N*-MeBHA through the following reaction mechanisms. Namely, a molecular complex has been located as the first step of the title reaction followed by the nucleophilic attack process, resulting in the formation of an unstable intermediate containing N–O bond. Subsequently, the unstable intermediate decomposes homolytically *via* the cleavage of N–O bond to produce the N- and O-centered radicals. For the O-centered radical, it can easily isomerize to the C-centered radical. Finally, the C-centered radical reacts with the N-centered radical to produce the major C–N bonding product, accompanying with the formation of minor C–O bonding product. In addition, it was found that the reactivity of *o*-TCBQ with *N*-MeBHA is higher than that of *p*-TCBQ. Hopefully, the present results can provide helpful information for the detection and identification of the reaction products experimentally. Certainly, relevant experiments are required to further confirm the present results.

Acknowledgements

This work is supported by NSFC (21577076, 21303093, and 21003082) and the NSF of Shandong Province (ZR2014BM020).

References

1 J. L. Bolton, M. A. Trush, T. M. Penning, G. Dryhurst and T. J. Monks, *Chem. Res. Toxicol.*, 2000, **13**, 135–160.
2 Y. Song, B. A. Wagner, J. R. Witmer, H. J. Lehmler and G. R. Buettner, *Proc. Natl. Acad. Sci. U. S. A.*, 2009, **106**, 9725–9730.
3 B. Meunier, *Science*, 2002, **296**, 270–271.
4 S. S. Gupta, M. Stadler, C. A. Noser, A. Ghosh, B. Steinhoff, D. Lenoir, C. P. Horwitz, K. Schramm and T. J. Collins, *Science*, 2002, **296**, 326–328.
5 A. Sorokin, J. L. Seris and B. Meunier, *Science*, 1995, **268**, 1163–1166.
6 Y. L. Zhao, F. Qin, J. M. Boyd, J. Anichina and X. F. Li, *Anal. Chem.*, 2010, **82**, 4599–4605.
7 F. Qin, Y. Y. Zhao, Y. L. Zhao, J. M. Boyd, W. J. Zhou and X. F. Li, *Angew. Chem., Int. Ed.*, 2010, **49**, 790–792.
8 J. H. Li, W. Wang, B. Moe, H. L. Wang and X. F. Li, *Chem. Res. Toxicol.*, 2015, **28**, 306–318.
9 B. Z. Zhu, N. Kitrossky and M. Chevion, *Biochem. Biophys. Res. Commun.*, 2000, **270**, 942–946.
10 B. Z. Zhu, H. Zhao, B. Kalyanaraman and B. Frei, *Free Radical Biol. Med.*, 2002, **32**, 465–473.
11 B. Z. Zhu, B. Kalyanaraman and G. B. Jiang, *Proc. Natl. Acad. Sci. U. S. A.*, 2007, **104**, 17575–17578.
12 B. Z. Zhu and G. Q. Shan, *Chem. Res. Toxicol.*, 2009, **22**, 969–977.
13 B. Z. Zhu, L. Mao, C. H. Huang, H. Qin, R. M. Fan, B. Kalyanaraman and J. G. Zhu, *Proc. Natl. Acad. Sci. U. S. A.*, 2012, **109**, 16046–16051.
14 B. Z. Zhu, H. T. Zhao, B. Kalyanaraman, J. Liu, G. Q. Shan, Y. G. Du and B. Frei, *Proc. Natl. Acad. Sci. U. S. A.*, 2007, **104**, 3698–3702.
15 B. Z. Zhu, G. Q. Shan, C. H. Huang, B. Kalyanaraman, L. Mao and Y. G. Du, *Proc. Natl. Acad. Sci. U. S. A.*, 2009, **106**, 11466–11471.
16 C. H. Huang, F. R. Ren, G. Q. Shan, H. Qin, L. Mao and B. Z. Zhu, *Chem. Res. Toxicol.*, 2015, **28**, 831–837.
17 Y. Yu, J. Wong, D. B. Lovejoy, D. S. Kalinowski and D. R. Richardson, *Clin. Cancer Res.*, 2006, **12**, 6876–6883.
18 P. A. Marks and R. Breslow, *Nat. Biotechnol.*, 2007, **25**, 84–90.
19 N. N. Li, D. Zhao, M. Kirschbaum, C. Zhang, C. L. Lin, I. Todorov, F. Kandeel, S. Forman and D. F. Zeng, *Proc. Natl. Acad. Sci. U. S. A.*, 2008, **105**, 4796–4801.
20 B. Z. Zhu, J. G. Zhu, L. Mao, B. Kalyanaraman and G. Q. Shan, *Proc. Natl. Acad. Sci. U. S. A.*, 2010, **107**, 20686–20690.
21 B. Z. Zhu and C. H. Huang, *Free Radical Biol. Med.*, 2011, **51**, S152.

22 C. H. Huang, *Molecular mechanisms for novel radical and rearrangement reactions mediated by halogenated quinoid carcinogens*, University of Chinese Academy of Sciences, 2013.
23 B. S. Das, S. G. Reid, J. L. Betts and K. Patrick, *J. Fish. Res. Board Can.*, 1969, **26**, 3055–3067.
24 X. W. Guo and H. Mayr, *J. Am. Chem. Soc.*, 2014, **136**, 11499–11512.
25 S. Maddila, V. D. B. C. Dasireddy and S. B. Jonnalagadda, *Appl. Catal., B*, 2013, **138–139**, 149–160.
26 M. Freytag, P. G. Jones, R. Schmutzler and M. Yoshifuji, *Heteroat. Chem.*, 2001, **12**, 300–308.
27 M. Kot and W. Zaborska, *J. Enzyme Inhib. Med. Chem.*, 2006, **21**, 537–542.
28 H. R. Zare, M. Eslami, M. Namazian and M. L. Coote, *J. Phys. Chem. B*, 2009, **113**, 8080–8085.
29 C. Guo, W. H. Wang, W. L. Feng and P. Li, *RSC Adv.*, 2017, **7**, 12775–12782.
30 P. Li, C. Guo, W. L. Feng, Q. Sun and W. H. Wang, *RSC Adv.*, 2017, **7**, 22919–22926.
31 P. Li, Z. Y. Ma, W. H. Wang, Y. Z. Zhai, H. T. Sun, S. W. Bi and Y. X. Bu, *Phys. Chem. Chem. Phys.*, 2011, **13**, 941–953.
32 W. L. Feng, C. Ren, W. H. Wang, C. Guo, Q. Sun and P. Li, *RSC Adv.*, 2016, **6**, 48099–48108.
33 L. M. Wang and A. L. Tang, *Chemosphere*, 2011, **82**, 782–785.
34 X. B. Wang, Q. Fu and J. L. Yang, *J. Phys. Chem. A*, 2010, **114**, 9083–9089.
35 S. L. Zhuang, H. F. Wang, K. K. Ding, J. Y. Wang, L. M. Pan, Y. L. Lu, Q. J. Liu and C. L. Zhang, *Chemosphere*, 2016, **144**, 1050–1059.
36 S. L. Zhuang, X. Lv, L. M. Pan, L. P. Lu, Z. W. Ge, J. Y. Wang, J. P. Wang, J. S. Liu, W. P. Liu and C. L. Zhang, *Environ. Pollut.*, 2017, **220**, 616–624.
37 P. Li, Z. T. Shen, W. H. Wang, Z. Y. Ma, S. W. Bi, H. T. Sun and Y. X. Bu, *Phys. Chem. Chem. Phys.*, 2010, **12**, 5256–5267.
38 W. L. Feng, C. Ren, W. H. Wang, C. Guo, Q. Sun and P. Li, *Theor. Chem. Acc.*, 2016, **135**, 190.
39 W. H. Wang, X. X. Zhang, P. Li, Q. Sun, Z. Li, C. Ren and C. Guo, *J. Phys. Chem. A*, 2015, **119**, 796–805.
40 C. Gonzalez and H. B. Schlegel, *J. Chem. Phys.*, 1989, **90**, 2154–2161.
41 C. Gonzalez and H. B. Schlegel, *J. Phys. Chem.*, 1990, **94**, 5523–5527.
42 S. F. Boys and F. Bernardi, *Mol. Phys.*, 1970, **19**, 553–566.
43 J. Tomasi, B. Mennucci and R. Cammi, *Chem. Rev.*, 2005, **105**, 2999–3093.
44 S. Miertuš, E. Scrocco and J. Tomasi, *Chem. Phys.*, 1981, **55**, 117–129.
45 H. B. Schlegel, J. M. Millam, S. S. Iyengar, G. A. Voth, A. D. Daniels, G. E. Scuseria and M. J. Frisch, *J. Chem. Phys.*, 2001, **114**, 9758–9763.
46 S. S. Iyengar, H. B. Schlegel, J. M. Millam, G. A. Voth, G. E. Scuseria and M. J. Frisch, *J. Chem. Phys.*, 2001, **115**, 10291–10302.
47 H. B. Schlegel, S. S. Iyengar, X. Li, J. M. Millam, G. A. Voth, G. E. Scuseria and M. J. Frisch, *J. Chem. Phys.*, 2002, **117**, 8694–8704.
48 M. J. Frisch, G. W. Trucks, H. B. Schlegel, G. E. Scuseria, M. A. Robb, J. R. Cheeseman, G. Scalmani, V. Barone, B. Mennucci, G. A. Petersson, H. Nakatsuji, M. Caricato, X. Li, H. P. Hratchian, A. F. Izmaylov, J. Bloino, G. Zheng, J. L. Sonnenberg, M. Hada, M. Ehara, K. Toyota, R. Fukuda, J. Hasegawa, M. Ishida, T. Nakajima, Y. Honda, O. Kitao, H. Nakai, T. Vreven, J. A. Montgomery Jr, J. E. Peralta, F. Ogliaro, M. Bearpark, J. J. Heyd, E. Brothers, K. N. Kudin, V. N. Staroverov, T. Keith, R. Kobayashi, J. Normand, K. Raghavachari, A. Rendell, J. C. Burant, S. S. Iyengar, J. Tomasi, M. Cossi, N. Rega, J. M. Millam, M. Klene, J. E. Knox, J. B. Cross, V. Bakken, C. Adamo, J. Jaramillo, R. Gomperts, R. E. Stratmann, O. Yazyev, A. J. Austin, R. Cammi, C. Pomelli, J. W. Ochterski, R. L. Martin, K. Morokuma, V. G. Zakrzewski, G. A. Voth, P. Salvador, J. J. Dannenberg, S. Dapprich, A. D. Daniels, O. Farkas, J. B. Foresman, J. V. Ortiz, J. Cioslowski and D. J. Fox, Gaussian, Inc., Wallingford CT, 2013.
49 P. Li, W. H. Wang, Q. Sun, Z. Li, A. J. Du, S. W. Bi and Y. Zhao, *ChemPhysChem*, 2013, **14**, 2737–2743.